PAPER

Check for updates

Strontium ranelate-loaded POFC/β-TCP porous scaffolds for osteoporotic bone repair

Caicai Ge, [b] Fangping Chen, [*ab] Lijie Mao,[b] Qing Liang,[b] Yan Su[*c] and Changsheng Liu [ab]

It is of considerable significance to fabricate scaffolds with satisfactory osteogenic activities and high osteogenesis quality to accelerate osteoporotic repair. In this study, we initially fabricated the POFC/β-TCP porous scaffold in the light of composition and structure bionics, and then loaded the SR to the optimized POFC/β-TCP porous scaffold by 3D printing based on FFS-MDJ. The hydrophilicity, mechanical properties biodegradability and cell response of the composite scaffolds were systematically investigated. The result showed that modified POFC enhanced the hydrophilicity and ameliorated the brittleness of pure β-TCP. β-TCP buffered the acidity and improved the degradability and cell affinity of the scaffold, and the release of strontium ranelate significantly promote the proliferation and differentiation of osteoblasts and guided bone regeneration. The results indicated that POFC/β-TCP scaffolds had uniform macropores of 300−500 μm and a porosity of approximately 48%, adjustable biodegradability and a high compressive modulus of 30−60 MPa. The strontium ranelate-loaded POFC/β-TCP scaffold enhanced the osteogenic differentiation of rBMSCs, which might be a promising candidate for osteoporotic-related bone defect repair.

1   Introduction

The exploding aging population, reduction of female estrogen levels with age, increased side effects of drugs and inflammatory factors trigger the sharp increased incidence of osteoporosis. The worldwide disability caused by osteoporotic fractures has accounted for 0.83% of non-communicable diseases. Globally, more than 200 million people suffer from osteoporosis.[1] Osteoporosis is a metabolic disease entailing a decrease in both bone density and quality, leading to fractures that frequently involve disability and even death.[2] Therefore, to fabricate scaffolds with satisfactory osteogenic activities and high osteogenesis quality are of considerable significance to accelerate osteoporotic repair and reduce complications and related healthcare costs.

The repair and treatment of osteoporotic bone fractures remain a clinical challenge. On one hand, the mesenchymal stem cells of osteoporotic bone have less capacity to differentiate into osteoblasts, together with a decreased angiogenic capacity at the defect site. On the other hand, scaffolds have to cope with the delayed bone healing and impair osseointegration. In this sense, association of antiosteoporosis drugs with scaffolds is a considerable strategy to accomplish rapid repair of osteoporotic fractures by regulating the osteoblastic bone formation and osteoclastic resorption at the injury site.

An ideal bone scaffold should possess excellent biocompatibility, good biodegradation, appropriate compressive strength and porous architecture. Sufficient porosity, tunable pore sizes and pore connectivity for oxygen and nutrients transport are conducive to guide cells to the defect site, limit cell loss and promote tissue ingrowth.[3]

Freeform Fabrication System with Micro-Droplet Jetting (FFS-MDJ) is an effective 3D printing technique where materials are used as 'ink' to fabricate scaffolds.[4,5] FFS-MDJ can construct controllable pore sizes and complex structures for cell migration, proliferation, and promote the high diffusion of nutrients and metabolites required for tissue regeneration.[6–8]

Beta-tricalcium phosphate (β-TCP) with high bioactivity and excellent osteoconductivity is used clinically for bone repair.[9–11] However, the drawbacks such as low compressive strength[12] and molding difficulty impede the further application in load-bearing bone reconstruction.[13] Unfortunately, the acidic degradation products of the polymers and the acidity accumulation tend to induce bacteria-free inflammation.[14] Therefore, the combination of β-TCP with polymers is an alternative strategy to improve mechanical strength, neutralize the acidity and enhance the hydrophilicity of the scaffold.

aKey Laboratory for Ultrafine Materials of Ministry of Education, School of Materials Science and Engineering, East China University of Science and Technology, Shanghai 200237, P. R. China. E-mail: fpchen@ecust.edu.cn; Fax: +86-21-64251358; Tel: +86-21-64251308

bEngineering Research Center for Biomedical Materials of Ministry of Education, East China University of Science and Technology, Shanghai 200237, P. R. China. E-mail: gecaicai123@163.com

cDepartment of Orthopedics, Affiliated Sixth People's Hospital, Shanghai Jiaotong University, Shanghai 200032, China. E-mail: 2536657535@qq.com

Citric acid is naturally abundant in bone tissue, and plays a vital role in bone metabolism and bone formation as an intermediate in the Krebs cycle.[15] Citrate upregulates C2C12 myoblasts and human mesenchymal stem cells osterix, alkaline phosphatase and osteopontin, while downregulates osteocalcin gene expression.[16] Furthermore, citrate can induce hydroxyapatite (HA) formation in simulated body fluid (SBF) and widely used in bone repair.[17,18] As one of citrate-based elastomers, poly(1,8-octanediol-co-citrate) (POC) has been developed and used in small-diameter vascular grafts, cartilage regeneration and bone regeneration.[18] POC displays excellent elasticity, controllable biodegradation and acceptable biocompatibility, but it is poor in hydrophilicity and degradability.[19] Good hydrophilicity is conducive to protein adsorption and cell adhesion. On the contrary, the absence of hydrophilicity will delay the degradation of materials.

Pluronic F127 is a water-soluble amphiphilic triblock copolymer of polyethylene glycol and polypropylene glycol and can be used as a hydrophilic polymer additive.[20,21] To further improve the hydrophilicity and degradability of citrate-based polymers, F127 was introduced to POC network as hydrophilic segment to tune the hydration, a new poly(1,8-octanediol-co F127 citrate) POFC with good hydrophilicity was synthesized in our study.

More importantly, the imbalance between diminished osteogenesis and excessive bone remodelling is a leading cause of bone defect repair caused by osteoporosis, which is quite different from conventional bone defects. High hydrophilicity and pore structure can promote osteoblast growth, accelerate nutrient transportation and vascularization, which is beneficial to bone repair. However, it is unable to inhibit osteoclast formation and regulate the balance between osteoblasts and osteoclasts.

Strontium ranelate (SR) has received an extensive attention due to its excellent physicochemical and pharmacokinetic characteristics.[22] SR has been used as an antiosteoporosis drug during the past 10 years. More interesting, SR simultaneously accelerates the osteoblast differentiation and inhibits the osteoclast formation.[23] SR significantly improves bone mass and increases bone strength by changing bone matrix and bone mineral density of patients.[24,25] Furthermore, SR was reported to remarkably reduce the fractures risk of spine or hip.[26] SR activated osteogenic differentiation of bone marrow stromal cells by activating cyclo-oxygenase 2 (COX-2) mediated prostaglandin E2. In addition, SR upregulated osteoprotegerin (OPG) and decreased receptor activator of nuclear factor kappa B (RANK) ligand expression in human osteoblastic cells, indicating that strontium ranelate reduced bone resorption by modulating the RANK/RANK-ligand/OPG system.[27,28] Therefore, if SR is loaded into POFC/β-TCP, the porous scaffolds will not only guide bone regeneration but also sustained release SR to promote osteogenic proliferation and differentiation of HMSCs. However, SR tended to treat the osteoporosis and fracture prevention just by oral administration, which greatly limits drug availability and its clinical application. Thereby, we anticipate that porous drug-loaded scaffolds could be constructed by incorporating SR into POFC/β-TCP *via* 3D printing. Thus, the question is whether SR has a therapeutic effect on osteoporosis and whether drug-loaded scaffolds have better repair effect on defects?

Herein, to promote the rapid repair and endow the drug curative effect on osteoporotic defects, we initially fabricated the POFC/β-TCP porous scaffold in the light of composition and structure bionics, and then loaded SR to the optimized POFC/β-TCP porous scaffolds. Furthermore, biodegradability, hydrophilicity and mechanical properties of the scaffolds were evaluated. Moreover, the effect of SR contents in the scaffolds on the osteogenic proliferation and differentiation expression of BMSCs *in vitro* was explored by ALP activity assay, mineralization staining and real-time PCR.

2 Experimental

2.1 Materials

Citric acid, 1,8-octanediol (99%), calcium hydroxide ($Ca(OH)_2$) and orthophosphoric acid (H_3PO_4) were purchased from Sinopharm Group Co. Ltd (Shanghai, China). Strontium ranelate was purchased from MACKLIN. PluronicF127, dimethyl sulfoxide (DMSO), 3-(4,5-dimethylthiazol-2-yl)-2,5-diphenylterazolium bromide (MTT) was purchased from Sigma-Aldrich (CA, USA). Fetal bovine serum and α-MEM culture medium were purchased from Gibco (Thermo Fisher Scientific., MA, USA) and HyClone (GE Healthcare, UK) respectively. BCA protein assay kit was purchased from Beyotime Biotech (Jiangsu, China). Reagents were all used without further purification.

2.2 Preparation and characterization of β-TCP and POFC

β-TCP was synthesized with calcium hydroxide ($Ca(OH)_2$) and orthophosphoric acid (H_3PO_4) solution. $Ca(OH)_2$ solution was added dropwise to the H_3PO_4 aqueous solution and kept stirring for 5 h. The precipitates were obtained *via* centrifugation and freeze-dried for 24 h. After sintering at 900 °C for 2 h, the dried powders were ground and sieved through 400 meshes, and then β-TCP powders with particle diameter less than 38.5 μm were obtained. The phase structure and composition of β-TCP were characterized by X-ray diffraction (XRD; D/Max-2550 V diffractometer; Rigaku Co., Japan) in a continuous scan mode and energy dispersive spectroscopy (EDS; JEOL JSM-6310LV; JEOL Ltd, Japan).

POFC was prepared by POFC pre-polymers (pre-POFC) and F127, according to Wang's method.[19] In brief, citric acid anhydrous, 1,8-octanedio and F127 was added to 500 mL three-necked flask, heated at 165 °C and stirred for 15 min under N_2 atmosphere. The mixture reacted at 140 °C until pre-POFC with suitable molecular weight was produced. The pre-POFC was dissolved and precipitated in ethyl alcohol. After washing and purification, the precipitates were freeze-dried and then insulated at 80 °C for 3 days for further chemical crosslinking. The as-prepared POFC was characterized by Fourier transform infrared spectroscopy (FTIR; Nicolet 5700; Thermo Ltd, USA) within the wavelength range of 4000 to 400 cm^{-1} at room temperature. The thermal properties were analyzed by differential scanning calorimeter (DSC; DSC-2910, TA).

2.3 Preparation of POFC/β-TCP

The POFC/β-TCP paste was prepared according to following procedures. The paste was formed by mixing POFC with β-TCP at different proportions, and then fed into the stainless-steel syringe in FFS-MDJ (Fuchi Co., Ltd, China) to fabricate square block samples ($10 \times 10 \times 4$ mm^3 and $10 \times 10 \times 2$ mm^3). Table 1 listed the weight ratios of POFC to β-TCP powders. The contents of POFC as were 25%, 35% and 45% respectively. The scaffolds were printed layer-by-layer according to the predefined pattern with a set layer thickness of 0.4 mm. Ultimately, the POFC/β-TCP scaffolds were prepared by polymerizing 3 days at 80 °C.

2.4 Characterization of POFC/β-TCP scaffolds

2.4.1 FTIR and TGA. FTIR recorded infrared spectra of scaffolds within the wavelength range of 4000 to 400 cm^{-1} at room temperature. Thermogravimetric analysis (TG; STA409PC; NETZSCHT Ltd., Germany) was performed on all scaffolds from room temperature to 800 °C at the heating rate of 10 °C min^{-1} under nitrogen atmosphere.

2.4.2 Surface morphology and porosity. The macroporous structure and micromorphology of the composite scaffolds were investigated by a field emission scanning electron microscope (FESEM, Hitachi S-4800). The porosity of POFC/β-TCP was evaluated by ethanol infiltration method. The initial weight of POFC/β-TCP scaffolds ($10 \times 10 \times 4$ mm^3) was marked as W_0. The weight of the bottle filled with ethanol was marked as W_1. The scaffolds were immersed into ethanol and the total weight (W_2) of the ethanol, ethanol-penetrated scaffolds and bottle was recorded. The lengths (l), width (w), and height (h) were measured. ρ presents the density of ethanol at room temperature. The porosity of scaffolds was calculated according to formula (1):

$$\text{Porosity } (\%) = 1 - (W_1 - W_2 + W_0)/\rho/(l \times w \times h) \tag{1}$$

2.4.3 Hydrophilicity and the mechanical properties. The hydrophilcity of POFC/β-TCP scaffolds ($10 \times 10 \times 2$ mm^3) was evaluated every 10 s by the water contact angle (Contact Angle System, JC2000D; Zhongchen Co., Ltd) at 25 °C. The mechanical properties of scaffolds ($10 \times 10 \times 4$ mm^3) with different contents of POFC were tested using a standard compression test (INSTRON Ltd., USA) at a compression speed of 1 mm min^{-1}. Three samples of each scaffold were tested.

2.4.4 In vitro degradation. The in vitro degradation of scaffolds was characterized by the weight loss ratio at different time intervals. POFC/β-TCP scaffolds ($10 \times 10 \times 2$ mm^3, weight G_1)

were soaked in Tris–HCl buffer solution (pH = 7.4) at the ratio of 0.1 g/20 mL at 37 °C for 10 weeks. The Tris–HCL was replaced every three days. At the pre-set time, each sample was washed, dried and recorded as final weight of G_2. The weight loss was expressed as the percentage of the initial weight by a formula ($G_1 - G_2$)/$G_1 \times 100\%$. TGA evaluated the weight loss ratios of each component (β-TCP and POFC) and SEM observed the scaffold surface.

2.4.5 Cell compatibility. The cell compatibility (including cell attachment and proliferation) of POFC/β-TCP scaffolds ($10 \times 10 \times 2$ mm^3) was assessed by rat bone marrow stem cells (rBMSCs). rBMSCs were isolated from rat bone marrow of tibia and femur, approved by the Research Center for Laboratory Animals of Shanghai University of Traditional Chinese Medicine. The bone marrow was flushed out with α-MEM loading 10% fetal bovine serum (FBS) and 1% antibiotics (100 U mL^{-1} penicillin G and 100 μg mL^{-1} streptomycin sulphate). The bone marrow suspension in a culture flask was incubated at 37 °C with 5% CO$_2$. rBMSCs obtained from 2 or 3 passages were utilized.

For cell attachment characterization, rBMSCs were seeded on the POFC/β-TCP scaffolds at a density of 1.0×10^5 cell per well in a 24-well cell culture plate and then incubated at 37 °C in an atmosphere of 5% CO$_2$. After 24 h incubation, samples were washed with PBS and fixed with 2.5% glutaraldehyde solution for 15 min at 4 °C. The fixed cells were washed with PBS twice and dehydrated with a series of ethanol solution (30, 50, 70, 80, 90, and 100%, v/v) for 5 min. The cell morphologies were visualized via SEM. Cellular compatibility and proliferation were evaluated by MTT assay. Briefly, rBMSCs were seeded on the POFC/β-TCP scaffolds at a density of 1.0×10^5 cell per well in 24-well culture plates. After incubation for 1, 3, and 7 d, 100 μL MTT solution (5 mg mL^{-1}) was added and incubated at 37 °C for 4 h. The numbers of cells were measured according to the optical density (OD) of the chromophore at 492 nm with a microplate reader (Spectra Max M2; Molecular Devices, USA).

2.5 Strontium ranelate loaded into and released from POFC/β-TCP

Strontium ranelate (SR) loaded scaffolds were fabricated with 35% POFC/β-TCP as matrix. The POFC/β-TCP scaffolds with 10% (w/w) SR were named 10SR/POFC/β-TCP. Ingredients were blended evenly to print. The SR-loaded scaffold ($10 \times 10 \times 2$ mm^3) were printed as pure POFC/β-TCP scaffold described above and post-polymerized at 80 °C for 3 days. The infrared spectra of the SR-loaded scaffolds were recorded by FTIR.

Table 1 Compositions, porosity, water contact angle, and compressive modulus of POFC/β-TCP scaffolds

Samples	POFC (wt%)	β-TCP (wt%)	Porosity (%)	Water contact angle (°)	Compressive modulus (MPa)
25% POFC	25	75	48.15 ± 0.45	57.9 ± 3	47.82 ± 4.33
35% POFC	35	65	47.78 ± 2.12	58.9 ± 2	62.33 ± 5.30
35% POFC	45	55	49.23 ± 3.52	66.1 ± 5	27.17 ± 3.70

The SR-loaded scaffolds ($10 \times 10 \times 2$ mm^3) were soaked in PBS (0.01 M, pH = 7.2) at the ratio of 0.1 g/20 mL and kept shaking (80 rpm) in an incubator at 37 °C. 3 mL solution was replaced by an equal amount of fresh PBS every set interval. The released amount of SR was assayed *via* UV-vis spectrophotometer (SpectraMax M2; Molecular, USA) at 343 nm wavelength. SR in the buffer solution was collected every set interval and its concentration was calculated according to the standard curve.

2.6 Bioactivity of strontium ranelate loaded POFC/β-TCP

2.6.1 Cytotoxicity and cell proliferation. Cytotoxicity and cell proliferation on the scaffolds were assessed by the MTT assay. Briefly, rBMSCs were seeded on the POFC/β-TCP and SR/POFC/β-TCP scaffolds at a density of 1.0×10^5 cell per well in 24-well culture plates. After incubation for 1, 3, and 7 d, 100 μL MTT solution (5 mg mL^{-1}) was added and incubated at 37 °C for 4 h. The numbers of cells were measured according to the optical density (OD) of the chromophore at 492 nm with a microplate reader. Cells cultured directly on 24-well plate were used as control, and these experiments were performed in quadruplicates.

2.6.2 Alkaline phosphate (ALP) activity. ALP activity of rBMSCs was used to evaluate the early osteogenic differentiation of the cells on the scaffolds. rBMSCs were seeded on POFC/β-TCP and SR/POFC/β-TCP scaffolds at a density of 3×10^4 cells per well. After post-seeding for 24 h, the medium was replaced by osteogenic differentiation medium with 2% FBS, 100 nM dexamethasone, 0.05 mM ascorbic acid and 100 mM β-glycerol phosphate. After incubation for 4, 7 and 14 days, the medium of each well was removed and rBMSCs were washed three times with PBS. 500 μL Nonidet P-40 solution added to each well and incubated for 90 min at 37 °C. 50 mL cell lysates of each sample were placed in 96-well plates, and 200 mL of 1 mm g mL^{-1} pNPP was added and then incubated for 2 h at 37 °C. The reaction was quenched by 100 μL of 0.1 mol L^{-1} NaOH. ALP activity was quantified by a microplate reader at 405 nm. The total protein content was determined using a BCA protein assay kit. Meantime, the ALP staining was carried out at day 7. The POFC/β-TCP and SR/POFC/β-TCP scaffolds were stained in blue-purple by BCIP/NBT assay. The more blue-purple areas covers, the higher ALP activity and the more excellent osteogenic differentiation are. The cells were washed three times with PBS, and cells were observed by an inverted microscope (TE2000U, Nikon Corp, Japan).

2.6.3 Mineralization. Mineralization of rBMSCs was analyzed using alizarin red staining (ARS) on day 7, which assessed the calcium deposition by cells incubated on scaffolds. After incubation, cells were washed with PBS and fixed with 2.5% glutaraldehyde solution. The fixed cells were stained with 1% alizarin red (pH = 4.2) for 2 h at 37 °C. Subsequently, the stained scaffolds were washed with PBS and observed. Deeper red-purple areas meant more calcium depositions.

2.6.4 Real-time quantitative polymerase chain reaction (RT-qPCR) analysis. Osteogenic relative gene expressions were assessed by RT-qPCR (Bio-Rad, Hercules, CA, USA). rBMSCs were seeded respectively on the POFC/β-TCP and SR/POFC/β-TCP scaffolds for 7 and 14 days. Osteogenic differentiation markers: alkaline phosphatase (ALP), bone sialoprotein (BSP), Col 1, osteocalcin (OCN) and runt-related transcription factor 2 (Runx2) were bought commercially (Shengong, Co. Ltd. Shanghai, China). β-Actin gene was used as a housekeeping gene. All relative gene expression levels were normalized to β-actin. All experiments were performed in quadruplicates.

Primer sequences were as follows:

β-Actin forward 5′-CACCCGCGAGTACAACCTTC-3′, reverse 5′-CCCATACCCACCATCACACC-3′; RUNX2 forward 5′-ACCAGC-CACCTTTACTTACACC-3′, reverse 5′-GGTACCATTGGGAACTGA-TAGG-3′; ALP forward 5′-CGGAAGTGAGGCAGGTAG-3′, reverse 5′-AGAGCCCACAATGGACAG-3′; COI-1 forward 5′-TGGACGGC-TGCACGAGT-3′, reverse 5′-TTGGGGTGGAGGGAGTTTA-3′; OCN forward 5′-GCCCTGACTGCATTCTGCCTCT-3′, reverse 5′-TCAC-CACCTTACTGCCCTCCTG-3′; BSP forward 5′-ACAGCT-GACGCTGGAAAGTTG-3′, reverse 5′-ACCTGCTCATTTTCATCC-ACTTC-3′.

2.7 Statistical analysis

The data were expressed as mean ± standard error. All data were collected from at least three parallel experiments. Statistical analysis was carried out using one-way analysis of variance (ANOVA). A *p*-value of <0.05 was considered statistically significant.

3 Results and discussion

3.1 Characterization of β-TCP and POFC polymer

Fig. 1(A) showed XRD patterns of β-TCP. The XRD spectra confirmed that the prepared powder was pure β-TCP according to JCPDS 09-0169. EDS (Fig. 1(B)) revealed that the molar ration of calcium to phosphorus was about 1.5. The FTIR analysis of poly(diol citrate) elastomers was shown in Fig. 1(C). The peaks
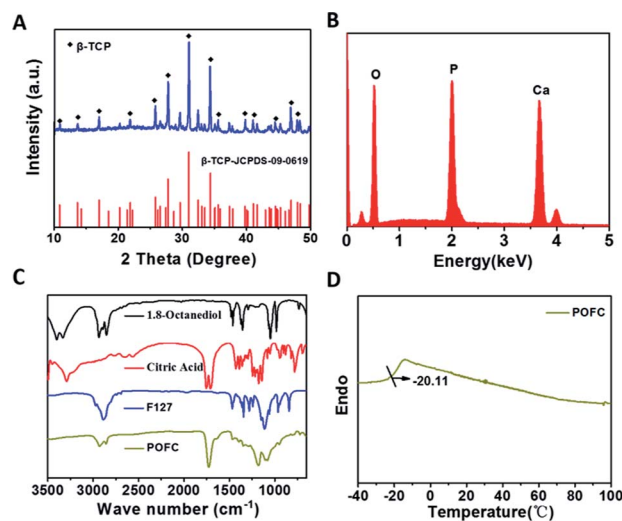

Fig. 1 (A) XRD patterns of β-TCP; (B) EDS patterns of β-TCP. (C) FT-IR spectra of POFC, 1,8-octanediol, citric acid and F127. (D) DSC curve of POFC.
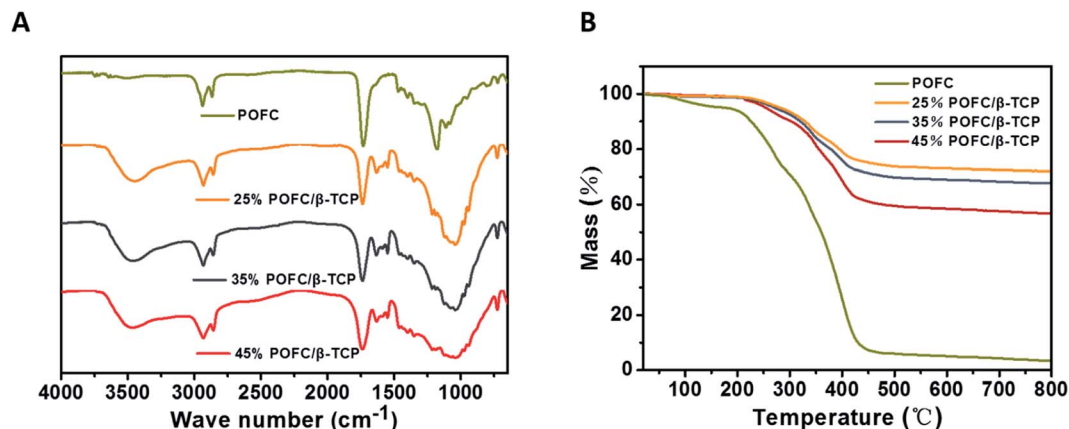
Fig. 2 (A) FTIR of POFC and POFC/β-TCP composite scaffolds with different POFC contents; (B) TGA curves of the POFC and POFC/β-TCP composite scaffolds with different POFC contents.

around 1690–1750 cm^{-1} represented the presence of carbonyl (C=O) groups.[18] Similarly, the peaks at 2940 and 2880 cm^{-1} were assigned to the asymmetrical and symmetrical stretching vibration of the –CH$_2$ groups in the spectra of POFC elastomer and 1,8-octanediol, which represented the methylene groups of 1,8-octanediol.[18] The peak at 1722 cm^{-1} originated from the carbonyl stretching vibration, which indicated successful polymerization of polyester groups. Two peaks at 1105 and 945 cm^{-1} appeared in POFC, which were attributed to the vibrations of C–O–C. It implied that F127 was involved in the network structure. DSC measured the glass transition temperature (T_g) of POFC. The result showed that no obvious crystallization or melting peaks in the curve (Fig. 1(D)). T_g of POFC was below 0 °C, no melting peaks or crystallization peaks were found, indicating that the synthetic polymer was amorphous at room temperature.

3.2 Characterization of POFC/β-TCP

3.2.1 Physicochemical properties of POFC/β-TCP. Fig. 2(A) displayed FTIR spectra of POFC and POFC/β-TCP. The characteristic peaks occurred in POFC/β-TCP, representing the interactions between POFC and β-TCP. The absorption peak at 1174 cm^{-1} was assigned to C–O vibrations. The peak at 1722 cm^{-1} was due to the carbonyl stretching vibration, which indicated successful polymerization of ester groups. Peaks at 2940 and 2880 cm^{-1} were assigned to the asymmetrical and symmetrical stretching vibration of –CH$_2$ groups, which were in all spectra of elastomers. The peak at 1092 cm^{-1} corresponded to the vibrations of C–O–C of F127. The bands, centered at 1023 cm^{-1} corresponding to the P–O bond, were found in POFC/β-TCP scaffolds. The results showed that the existence of β-TCP, and no other absorption peaks were detected in POFC/β-TCP.

Fig. 2(B) displayed the thermal stability of pure POFC and POFC/β-TCP. The results showed pure POFC had a complete weight loss of 97.3% and occurred thermal decomposition at 700 °C. Thermal decomposition temperature of all POFC/β-TCPs varied during the range of 210 °C and 600 °C. The thermal stability of POFC/β-TCP scaffolds was enhanced with the
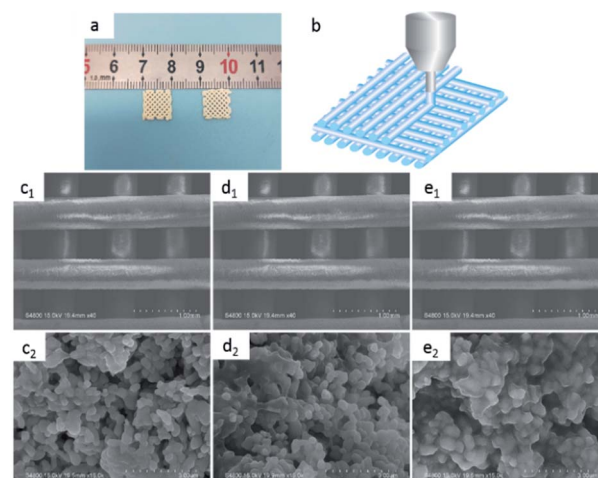

Fig. 3 (a) A photograph of 3D printing POFC/β-TCP scaffold; (b) scaffolds were fabricated via FFS-MDJ printing of the prepared inks; (c–e) SEM images of POFC/β-TCP composite scaffolds at different magnifications; (c1–e1) 40×; (c2–e2) 15 000×: (c1 and c2) 25% POFC/β-TCP, (d1 and d2) 35% POFC/β-TCP, (e1 and e2) 45% POFC/β-TCP.

increase content of β-TCP. 25% POFC/β-TCP, 35% POFC/β-TCP and 45% POFC/β-TCP lost weight of 24.8%, 32.2% and 43.21% respectively. The amounts of POFC (25%, 35%, and 45%) were in accordance with the weight loss of composite scaffolds. In addition, the mass loss of POFC/β-TCP scaffolds was positively correlated with the content of POFC in the scaffold. The results showed that the POFC/β-TCP scaffolds with the highest thermal stability correspond to the highest concentration of β-TCP in the scaffold.

3.2.2 Morphologies of POFC/β-TCP. The POFC/β-TCP pastes were extruded continuously and homogeneously through FFS-MDJ. Fig. 3 depicted the pore structure, morphology and microstructure of the scaffolds with different contents of POFC. The inner pore shapes of the POFC/β-TCP scaffold were controlled by regulating the angle of the process pattern. As seen in Fig. 3(c1–e1), the macrospore was 300–400 μm and was

completely connected. Moreover, the scaffolds were printed regularly with a crossing angel of 90°, which enhance the mechanical strength. Fig. 3(c2–e2) showed all surfaces of scaffolds at high magnification were porous and rough, which are helpful to promote cell adhesion and protein adsorption. The β-TCP nanoparticles were embedded in POFC polymer, and some agglomerations between nanoparticles were apparent. With the increase content of POFC, more β-TCP nanoparticles were embedded, which helps to overcome the brittleness of β-TCP and reinforce the POFC/β-TCP scaffold.

3.2.3 Contact angle and porosity. Contact angles were measured to evaluate the surface wettability of the composite. The hydrophilicity of scaffolds plays a crucial role in cell affinity and protein adsorption. Table 1 summarized the water contact angles of the scaffolds. The results indicated that all scaffolds were hydrophilic. On one hand, the introduction of F127 enhanced the hydrophilicity of the POFC elastomers. On the other hand, POFC contains a lot of hydrophilic hydroxyl, carboxyl and ether bonds. All these endowed the composite scaffolds low contact angle about 58°. The 25% POFC, 35% POFC and 45% POFC scaffolds were similar in porosities. Obviously, the contents of POFC had no influence on the porosity of scaffolds.

3.2.4 Mechanical properties. Mechanical strength of the scaffold is critical for bone repair. The scaffold should sustain external stress and match the growth rate of new tissues. Fig. 4 plotted compressive stress–strain curves of scaffolds. POFC/β-TCP had higher compressive modulus than that of pure β-TCP. Fig. 4(A) showed that the cross-linking of POFC with β-TCP made the polymer network tougher. Moreover, with the increase content of POFC, the compressive modulus of the POFC/β-TCP increased initially and then decreased (Fig. 4(B)). 45% POFC scaffold had the lowest compressive modulus of 27.17 ± 3.70 MPa. 25% POFC and 35% POFC scaffolds had

mean compressive modulus of 47.82 ± 4.33 MPa and 62.33 ± 5.30 MPa respectively. The compressive modulus of human trabecular bone range was between 2–12 MPa.[30] Fig. 4(C) indicated that pure β-TCP broke into fragments while POFC/β-TCP scaffolds remained an integrated structure. The result showed that the prepared POFC/β-TCP met the mechanical strength need for bone repair.

3.2.5 Degradation properties. An ideal scaffold should have the degradation rate matching the new bone formation. Fig. 5(A) presented the degradation of POFC/β-TCP with different contents of POFC. The result showed that POFC/β-TCP scaffolds with different contents of POFC had different degradation behaviours. It was obvious that all POFC/β-TCP scaffolds kept degrading during the entire incubation period. The degradation rate of POFC/β-TCPs increased with the increase content of POFC. POFC/β-TCP scaffolds with 35% POFC and 45% POFC showed higher weight loss, having similar degradation rates of 20% and 21.67% respectively after degradation for 10 weeks. On the contrary, POFC/β-TCP with 25% POFC had lower degradation rate of 14.5%. The result proved that the different degradation properties of POFC/β-TCP scaffolds related to hydrophilic and their composition.

To further study the degradation behaviour of the two components (β-TCP and POFC), the total weight loss of POFC/β-TCP scaffold was set as 100%. The weight loss ratios of β-TCP and POFC were calculated (Fig. 5(D)). Scaffolds with 25%, 35% and 45% β-TCP had weight loss ratio of 31.85%, 21.28% and 14.30% respectively. Meanwhile the scaffolds containing 25%, 35% and 45% POFC had weight loss ratios of 68.15%, 78.72% and 85.70%. The weight loss ratio of the composite scaffolds improved with the increased content of POFC while declined with the increased content of β-TCP. The scaffold with 45% POFC had a higher degradation ratio than the other two
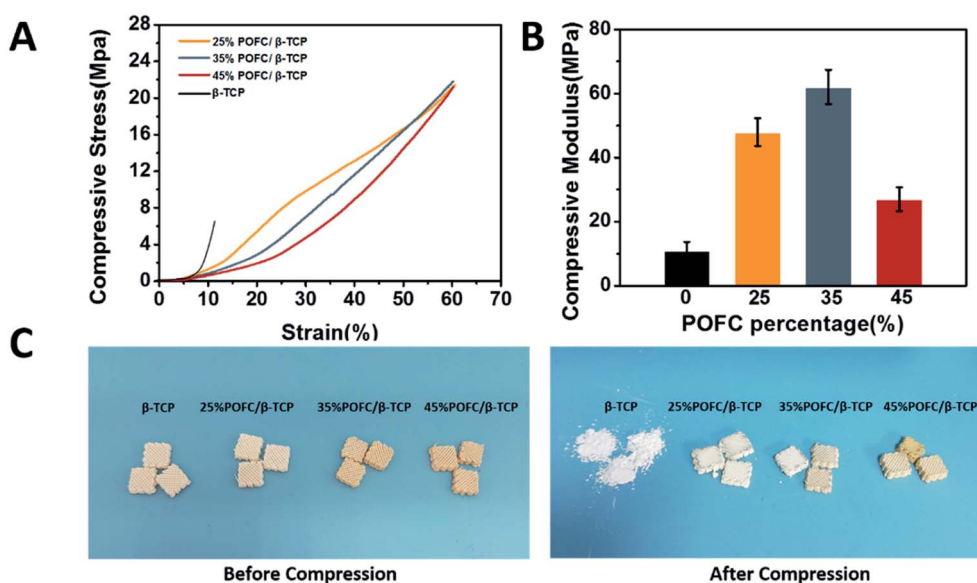

Fig. 4 (A) Typical stress–strain curves of the β-TCP scaffold and β-TCP/POC scaffolds with different POFC contents. (B) Compressive modulus of β-TCP/POC scaffolds with different POFC contents. (C) Photos of scaffolds before and after the compression test. Addition of POFC had improved the mechanical strength, solved the problem of brittleness of β-TCP scaffold.
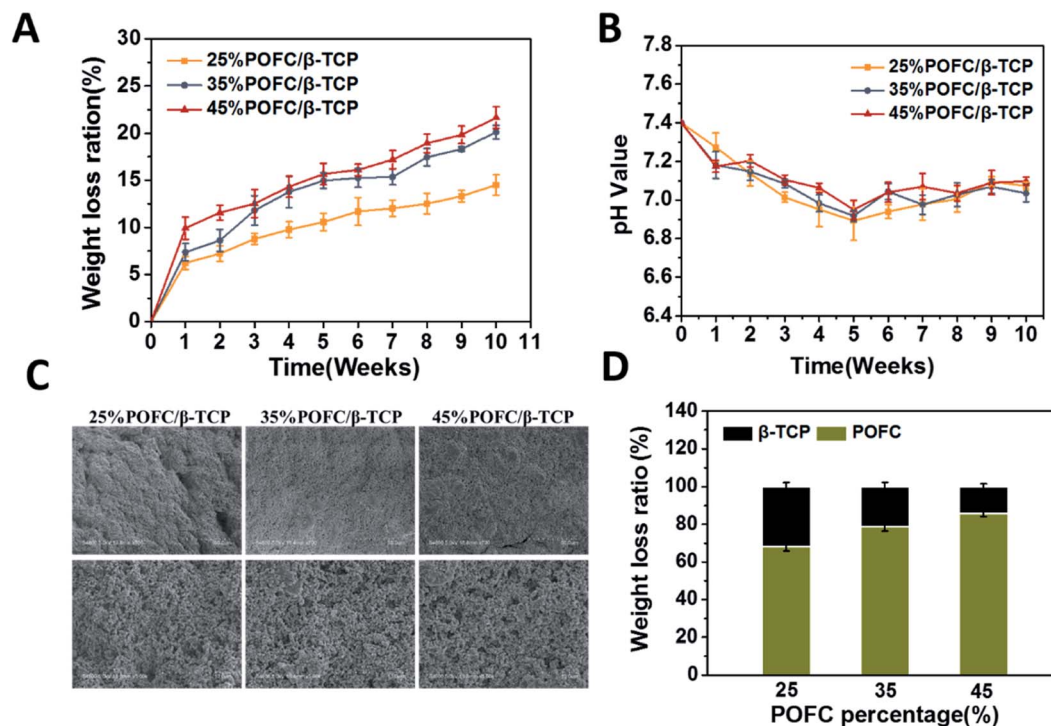
Fig. 5 (A) *In vitro* biodegradation curves of the β-TCP/POFC scaffolds; (B) pH value change of Tris−HCL buffer after immersing the β-TCP/POFC scaffolds; (C) SEM images of composite scaffolds with degradation time of 10 weeks. First row: 700× , second row: 5000×; (D) weight loss ratio of β-TCP and POFC in scaffolds at week 10.

scaffolds. The results showed that the degradation ratio can be regulated by the ratio of β-TCP and POFC.

The degradation of polymers was accompanied by acid problems. It was especially important to regulate the pH of degradation process. pH was measured during the degradation period in this study. As recorded in Fig. 5(B), scaffolds with different POFC contents remained acidic, mainly due to the citric acid release from POFC. β-TCP degraded and provided weak alkaline environment to neutralize acid. pH of the scaffolds reached a steady level at the sixth week. The result indicated that the introduction of β-TCP could effectively adjust the pH and kept stability of scaffolds.

Fig. 5(C) displayed SEM images of POFC/β-TCP scaffolds after degradation for 10 weeks. All samples displayed pore structure. With the degradation prolonged, more particles and cracks exposed on the surface of POFC. The scaffolds with 25% POFC formed the largest number of cracks. However, scaffolds with 35% and 45% POFC only contained a few polymer-coated inorganic particles, and most POFC were degraded, resulting in β-TCP exposure on the surface. Meanwhile, more POFC motivated itself to be degraded.

3.2.6 Cell attachment and proliferation. Cell morphology of rBMSCs on POFC/β-TCP scaffolds after culture for 24 h was observed by SEM (Fig. 6(A–C)). Cells were attached tightly on the surface and exhibited cellular morphology with extraordinary elongation of at least 40 μm. The numbers of cells on the POFC/β-TCP scaffolds with 25% and 35% POFC were much higher than the other.

Fig. 6(D) showed the rBMSCs proliferation on POFC/β-TCP scaffolds after 1, 3 and 7 days cell culture. The growth of rBMSCs *in vitro* was evaluated quantitatively with MTT assay. Cells proliferated with the time, which indicated that all materials had no influence on rBMSCs proliferation. The number of cells in 25% POFC/β-TCP and 35% POFC/β-TCP scaffolds increased, higher than that in the 45% POFC/β-TCP scaffolds. However, there is no statistical difference among
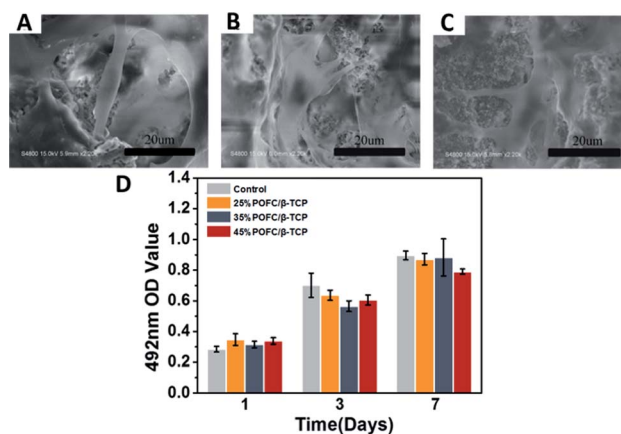

Fig. 6 (A–C) Morphologies of rBMSCs adhered on the β-TCP/POFC scaffolds surface after 24 h cultivation by SEM: (A) 25% POFC, (B) 35% POFC, and (C) 45% POFC. (D) Cell proliferation on β-TCP/POFC scaffolds cultured for 1, 3, and 7 d by MTT assay (experiments performed in quadruplicates).

different groups. The results indicated that all POFC/β-TCP scaffolds possessed excellent biocompatibility.

3.3 Strontium ranelate delivery and sustained release

Fig. 7(A) showed the FTIR spectra of the prepared scaffolds. Two new absorption peaks at 2220 cm^{-1} and 1579 cm^{-1} appeared with the addition of SR (10SR/POFC/β-TCP scaffold). The peak at 2220 cm^{-1} was due to the cyan bond stretching vibration of SR, and the peak at 1579 cm^{-1} was assigned to the stretching vibration of the carboxylic acid salt carbonic double bond in SR. These characteristic peaks indicated the interaction of SR with POFC/β-TCP. Fig. 7(B) showed SR released in a linear upward trend from the 10SR/POFC/β-TCP scaffold, while SR released 52.17% during the first 3 days and then reached the plateau. SR released 58.98% after 8 days. The sustained release of SR during 3–8 days was due to the swelling of POFC and high porosity of scaffolds. Therefore, the POFC/β-TCP scaffold was a promising carrier for sustained release SR.

3.4 Cytotoxicity and cell proliferation *in vitro*

Fig. 8 showed the rBMSCs proliferation on SR loaded scaffold after 1, 3 and 7 days cell culture. MTT assay evaluated the growth of rBMSCs *in vitro* quantitatively. As shown in Fig. 8, no cytotoxicity was observed on all scaffolds, and the number of cells in 10SR/POFC/β-TCP scaffolds was higher than that in the POFC/β-TCP scaffolds. The results indicated that 10SR/POFC/β-TCP possessed excellent biocompatibility and SR released from the 10SR/POFC/β-TCP scaffolds helped to promote stem cell proliferation which was consistent with previous literatures.

3.5 Osteogenic differentiation and gene expression

The osteogenesis of SR loaded scaffold was characterized by ALP activity, ALP staining, mineralization and expression of osteogenic differentiation markers. Osteogenic differentiation of rBMSCs seeded on the scaffolds is important to achieve successful bone repair. The ALP has been widely known as a marker of early osteoblastic differentiation. Fig. 9(A) displayed the ALP activity of rBMSCs cultured in POFC/β-TCP and 10SR/POFC/β-TCP scaffolds. The result showed that the addition of SR to POFC/β-TCP greatly increased the ALP activity compared with pure POFC/β-TCP. The ALP activity of 10SR/POFC/β-TCP was higher than that of the POFC/β-TCP group at day 4, day 7 and day 14. The ALP staining and ARS staining of rBMSCs cultured in
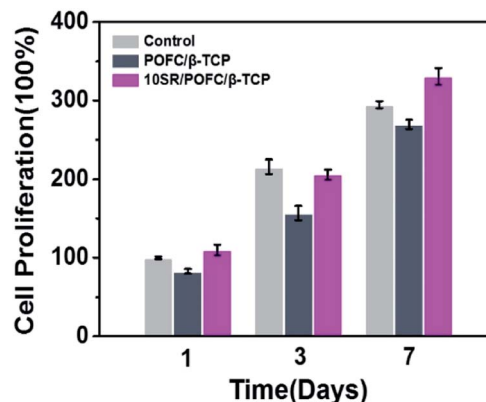

Fig. 8 Cell proliferation on POFC/β-TCP and 10SR/POFC/β-TCP scaffolds cultured for 1, 3, and 7 d by MTT assay (experiments performed in quadruplicates).

10SR/POFC/β-TCP extract were more intensive than those of POFC/β-TCP at day 14 (Fig. 9(B)). More importantly, the results were consistent with the ALP analysis results. Biomineralization was examined as a maker of fully differentiated cells at the stages of osteogenesis. Mineralized scaffolds were stained by alizarin red S dye. The stained 10SR/POFC/β-TCP exhibited darker colour than pure POFC/β-TCP. The result revealed the enhanced mineralization of 10SR/POFC/β-TCP (Fig. 9(B)).

The relative mRNA expression levels of the early osteogenesis related genes ALP, BSP, COL 1 and RUNX 2, and the late stage osteogenesis related genes OCN on day 7 and 14 were evaluated (Fig. 9(C)). RUNX 2 is known as a major gene in the osteoblast phenotype induction. It plays an important role in regulating osteogenic behaviour and promoting the upregulated of ALP, COL 1, BSP and OCN.[19] COL 1 is a key protein in bone matrix to promote osteogenic differentiation, matrix maturation and mineralization.[14] OCN regulates calcium ion concentrations during bone repair. These genes are upregulated due to osteoblastic differentiation of rBMSCs seeded on scaffolds.

It is quite interesting that the porous SR-loaded POFC/β-TCP scaffold significantly increased the gene expression of ALP, BSP, COL 1 and RUNX 2 of rBMSCs as assessed by real-time PCR at 7 and 14 days post-seeding, compared with that on pure POFC/β-TCP. Our study showed that the incorporation of SR into POFC/β-TCP scaffolds could enhance osteogenic proliferation and differentiation of rBMSCs. The result proved that the release of SR promoted stem cell osteogenesis in the 10SR/POFC/β-TCP scaffolds, which also confirmed in previous literatures.[29–31] SR loaded POFC/β-TCP inhibited the osteoclast formation and affected the osteogenic effect. Although previous studies indicated that SR stimulated proliferation and differentiation of BMSCs, few studies focused on the SR-incorporated scaffolds as an osteoporotic bone repair model. As concerned above, the combination of physicochemical and biological properties *in vitro* of 10SR/POFC/β-TCP scaffolds affirmed its feasibility for osteoporotic bone repair therapeutics. Further studies will conduct to investigate the underlying mechanism of bone formation and histological analyses of 10SR/POFC/β-TCP scaffolds *in vivo*.
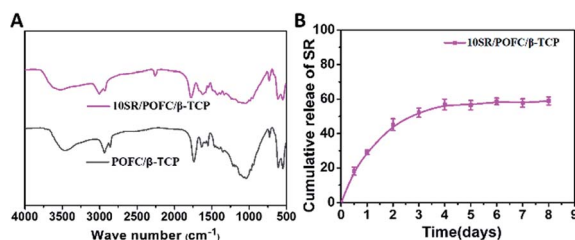

Fig. 7 (A) FTIR of β-TCP/POFC scaffold and SR loaded into β-TCP/POFC scaffold. (B) Cumulative release profiles of SR from β-TCP/POFC scaffold in PBS at 37 °C.
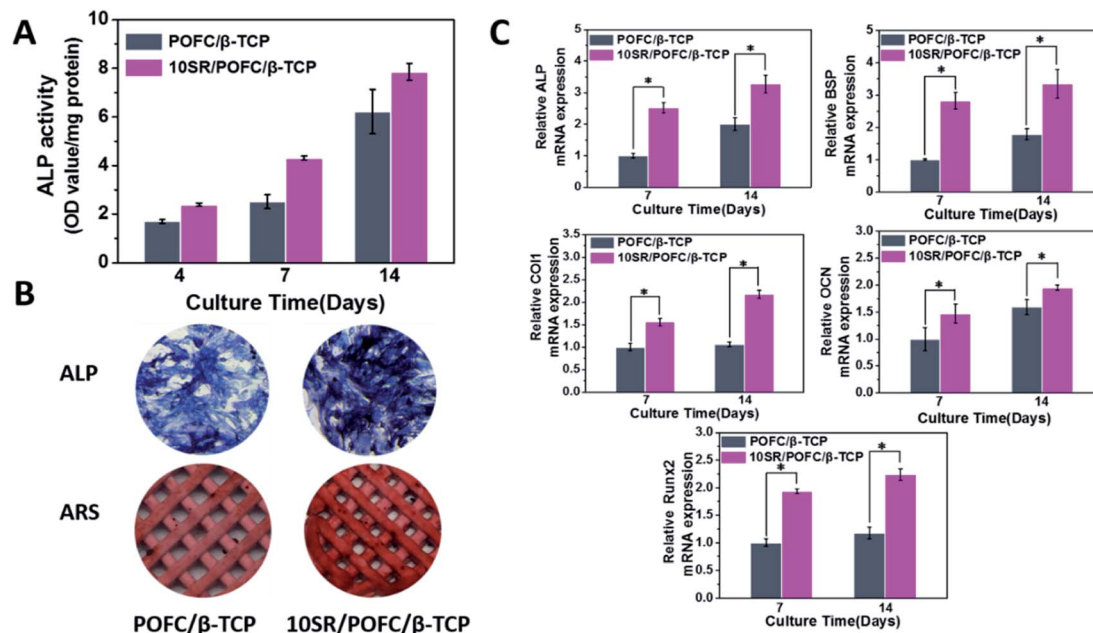
Fig. 9 Effects of SR loaded into β-TCP/POFC scaffold on estrogenic differentiation of rBMSCs. (A) ALP activity at day 7. (B) ALP staining (upper row) and ARS staining (bottom row) for 14 days. (C) Relative mRNA expression of osteogenesis-related gene in rBMSCs cultured on β-TCP/POFC and 10SR/β-TCP/POFC scaffolds. Gene expression of ALP, BSP, Col 1, OCN, and Runx2 were analyzed using RT-qPCR at 7 and 14.

4 Conclusions

Porous SR-loaded POFC/β-TCP scaffold was successfully fabricated *via* freeform fabrication system with micro-droplet jetting in the light of composition and structure bionics. The results indicated that 3D printed POFC/β-TCP scaffolds possess controllable pore structure, degradation ratio, hydrophilicity, excellent mechanical strength and biocompatibility. SR was successfully loaded and released from the POFC/β-TCP scaffold. MTT assay, ALP activity, calcium deposition and RT-qPCR analysis indicated that the SR loaded POFC/β-TCP scaffolds could promoted the proliferation and osteogenic differentiation of cell. As a whole, the combination of physicochemical and biological properties of SR-loaded POFC/β-TCP porous scaffolds demonstrated that SR loaded POFC/β-TCP scaffold is a potential candidate for bone defect repair in osteoporosis. Further studies will conduct to investigate the osteogenic ability of SR/POFC/β-TCP scaffold *in vivo*.

Conflicts of interest

There are no conflicts to declare.

Acknowledgements

References

1 O. Johnell and J. A. Kanis, *Osteoporosis Int.*, 2006, **17**, 1726–1733.
2 R. Burge, B. Dawson-Hughes and D. H. Solomon, *J. Bone Miner. Res.*, 2007, **22**, 465–475.
3 U. Aydemir Sezer, D. Arslantunali, E. A. Aksoy, V. Hasirci and N. Hasirci, *J. Appl. Polym. Sci.*, 2014, **131**, 40110–40119.
4 Q. A. Fu, E. Saiz and A. P. Tomsia, *Adv. Funct. Mater.*, 2011, **21**, 1058–1063.
5 C. Yang, X. Wang and B. Ma, *ACS Appl. Mater. Interfaces*, 2017, **9**, 5757–5767.
6 B. Piyush, R. M. Schweller, A. Khademhosseini, J. L. West and R. Bashir, *Annu. Rev. Biomed. Eng.*, 2014, **16**, 247–276.
7 S. P. Callahan, J. H. Callahan, C. E. Scheldegger and C. T. Silva, *Comput. Sci. Eng.*, 2008, **10**, 88–91.
8 Y. P. Chen and M. D. Yang, *Appl. Mech. Mater.*, 2014, **670**, 936–941.
9 Y. Tanimoto and N. Nishiyama, *J. Biomed. Mater. Res., Part A*, 2008, **85**, 427–433.
10 S. V. Dorozhkin and M. Epple, *Angew. Chem., Int. Ed.*, 2002, **41**, 3130–3146.
11 R. Z. Legeros, *Clin. Orthop. Relat. Res.*, 2002, **395**, 81–98.
12 P. Miranda, A. Pajares and E. Saiz, *J. Biomed. Mater. Res., Part A*, 2008, **85**, 218–227.
13 A. J. W. Johnson and B. A. Herschler, *Acta Biomater.*, 2011, **7**, 16–30.
14 Y. A. Fei, W. J. Cui and Z. Xiong, *Polym. Degrad. Stab.*, 2006, **91**, 3065–3073.
15 Y. Y. Hu, A. Rawal and K. Schmidt-Rohr, *Proc. Natl. Acad. Sci. U. S. A.*, 2010, **107**, 22425–22429.

16 R. T. Tran, L. Wang, C. Zhang, M. Huang and W. Tang, *J. Biomed. Mater. Res., Part A*, 2014, **102**, 2521–2532.

17 S. H. Rhee and J. Tanaka, *Biomaterials*, 1999, **20**, 2155–2160.

18 R. T. Tran, J. Yang and G. A. Ameer, *Annu. Rev. Mater. Res.*, 2015, **45**, 277–310.

19 J. Yang, A. R. Webb and S. J. Pickerill, *Biomaterials*, 2006, **27**, 1889–1898.

20 J. H. Lee, S. W. Kim and U. K. Kim, *J. Biomed. Mater. Res., Part A*, 2013, **101**, 942–953.

21 M. Kim, Y. Hwang and G. Tae, *Int. J. Biol. Macromol.*, 2016, **93**, 1603–1611.

22 J. Y. Reginster, M. P. Lecart, R. Deroisy and C. Lousberg, *Expert Opin. Invest. Drugs*, 2004, **3**, 857–886.

23 E. Bonnelye, A. Chabadel, F. Saltel and P. Jurdic, *Bone*, 2008, **42**, 129–138.

24 P. J. Marie, D. Felsenberg and M. L. Brandi, *Osteoporosis Int.*, 2011, **22**, 1659–1667.

25 S. Tenti, S. Cheleschi, G. M. Guidelli, M. Galeazzi and A. Fioravanti, *Mod. Rheumatol.*, 2014, **24**, 881–884.

26 J. Y. Reginster, D. Felsenberg, S. Boonen, A. Diez-Perez, R. Rizzoli, M. L. Brandi, T. D. Spector, K. Brixen, S. Goemaere, C. Cormier, A. Balogh, P. D. Delmas and P. J. Meunier, *Arthritis Rheuma*, 2008, **58**, 1687–1695.

27 E. Bonnelye, A. Lalande and P. Judric, *J. Bone Miner. Res.*, 2006, **21**, 426–434.

28 P. J. Marie, *Bone*, 2007, **40**, 5–8.

29 Y. Zhang, L. Wei, J. Chang, R. J. Miron, B. Shi and C. T. Wu, *J. Mater. Chem. B*, 2013, **1**, 5711–5722.

30 E. Bonnelye, A. Chabadel, S. Frédéric and J. Pierre, *Bone*, 2008, **42**, 129–138.

31 Z. Y. Mao, Z. W. Fang, Y. Q. Yang, X. Chen, Y. G. Wang, J. Kang, X. H. Qiu, W. E. Yuan and K. R. Dai, *RSC Adv.*, 2017, **7**, 24607–24615.